Electromagnetic Mechanism of SERS

George C. Schatz, Matthew A. Young, and Richard P. Van Duyne

Department of Chemistry, Northwestern University, Evanston,
IL 60208-3113, USA
{schatz,vanduyne}@chem.northwestern.edu

1 Introduction

Surface-enhanced Raman spectroscopy (SERS) was originally discovered in the 1970s [1, 2] where it was found that submonolayers of small nonresonant organic molecules, such as pyridine, when adsorbed onto the surface of silver nanoparticles (and a few other metals such as copper and gold) would exhibit greatly enhanced Raman intensities (enhancements of 10^6). These results have always held the promise for using this technique to observe very low concentrations of molecules on nanoparticles and nanostructured surfaces, but only recently has this promise started to be fulfilled in a predictable way. Thanks to exciting advances in techniques for making nanoparticles (such as nanosphere and e-beam lithography), to characterizing the surfaces using electron and scanning probe microscopies, to functionalizing the surfaces of the particles using self-assembled monolayers with attached chemical receptors, and to the laser and optics technology associated with measuring the Raman spectra, a number of important applications have been reported recently [3]. Included in these results have been the determination of SERS excitation spectra for benzenethiol on lithographically fabricated silver surfaces (periodic particle arrays fabricated using nanosphere lihtography) and the first observation of glucose using SERS [4, 5].

Another area of great interest in the SERS community concerns the observation of single-molecule SERS (SMSERS) [6, 7, 8]. This technique, which was originally developed in 1997 [6, 7], has proven to be of fundamental interest due to the nominal enhancement factor of $> 10^{13}$ required for the observation of any signal, but it has so far proven to be elusive in providing widespread applicability, due to the limited numbers of molecules and substrates for which successful observations have been made. In particular, almost all of the observations to date have been with molecules that are resonant Raman scatterers (such as rhodamine 6G), which typically have larger Raman intensities for non-SERS applications than nonresonant molecules like pyridine by factors of 10^4 or more. In addition, the range of substrates that yield SMSERS has been limited mostly to colloidal aggregate structures, which presumably are efficient at producing particle junction structures (i.e., dimers and small clusters of particles in which a molecule is sandwiched between the particles) that

K. Kneipp, M. Moskovits, H. Kneipp (Eds.): Surface-Enhanced Raman Scattering – Physics and Applications, Topics Appl. Phys. **103**, 19–46 (2006)
© Springer-Verlag Berlin Heidelberg 2006

are needed to produce the extraordinarily high enhancement factors required for SERS.

As noted above, SERS has almost exclusively been associated with three metals, silver (by far the most important), gold and copper. The generalization to other metals and other materials has been explored since the discovery of SERS, but only in the last few years have the tools been available to generate well-characterized experiments where the reported enhancements are reliable. An interesting result of recent work is that there is evidence that SERS can be observed for metals like rhodium [9, 10, 11, 12] and platinum [13,14,15,16,17,18,19] that are of key interest to the chemical industry through their importance in catalysis. Other metals, such as ruthenium [11] and aluminum [20] have a smaller literature, but remain of great interest due to their technological applications. The connection of these results with SERS-enhancement mechanisms is of great interest, but not yet established.

The last few years have seen several studies [21, 22, 23] aimed at using theory, particularly computational electrodynamics to provide a realistic, and even quantitative description of SERS. Much of this work originated with studies of extinction and scattering spectra, which led to an understanding of the dependence of the optical properties of metal nanoparticles on size, shape, arrangement and dielectric environment [24, 25, 26, 27, 28, 29, 30, 31, 32, 33, 34, 35, 36]. In addition, this work builds on earlier theory [37,38,39,40,41,42,43,44,45] in which the basic mechanisms of SERS were first postulated. This earlier work has been reviewed several times, [46,47,48] so we will only highlight a few studies. Although the idea that plasmon excitation would lead to enhanced Raman intensities even predates the discovery of SERS [49], and its possible role was pointed out in early theory papers [43,50], the first serious estimates of enhanced fields near metal nanoparticles were done in the late 1970s and early 1980s by *Gersten* and *Nitzan*, *Kerker* and others [40, 42, 51]. These calculations were based on simple models of the particle structures, such as spheres or spheroids, and some of the early estimates were not careful to distinguish the peak enhancement from average enhancement. A paper by *Zeman* and *Schatz* in 1987 [52] provided a detailed analysis of results for spheroids for many different metals. This work concluded that the average enhancement factor for silver was approximately 10^5 when optimized for particle size and shape. These conclusions were similar to those from the famous "posts" experiment at Bell labs [53], which for many years represented the only lithographically fabricated particles used in SERS experiments. However, the modeling of the posts was based on particle structures that were adjusted to match measured extinction spectra, so this did not represent an unparameterized comparison between theory and experiment.

In this Chapter we will review our recent studies of the electromagnetic mechanisms of SERS, including both experimental and computational studies. Our review begins with a discussion of the underlying theory of the electromagnetic mechanism along with a description of methods now used

to calculate fields. Then we consider a variety of issues that are important to the development of an understanding of SMSERS, including an analysis of SMSERS intensities for isolated particles, SMSERS for junctions between metal particles, and field enhancements arising from long-range electromagnetic interactions. In addition, we describe recent electronic structure studies that are aimed at developing a first-principles understanding of SERS. Our review concludes with a description of recent experimental studies using wavelength-scanned SERS excitation spectroscopy (WS SERES) to probe the electromagnetic mechanism.

2 Electromagnetic Mechanism of SERS

Since Raman intensities scale as the product of the incident field intensity and polarizability derivative, it comes as no surprise that there are two commonly considered mechanisms for SERS, one of which involves enhancements in the field intensity as a result of plasmon resonance excitation, and the other the enhancement in polarizability due to chemical effects such as charge-transfer excited states [40, 44, 46, 47, 54, 55, 56, 57]. The first of these is the well-known electromagnetic enhancement mechanism, and in this mechanism the enhancement factor E at each molecule is (approximately) given by

$$\mathsf{E} = |\boldsymbol{E}(\omega)|^2 |\boldsymbol{E}(\omega')|^2, \tag{1}$$

where $\boldsymbol{E}(\omega)$ is the local electric-field enhancement factor at the incident frequency ω and $\boldsymbol{E}(\omega')$ is the corresponding factor at the Stokes-shifted frequency ω'. More rigorous expressions for the electromagnetic enhancement factor, that do not involve a product of fields at different frequencies, have been given by *Kerker* [58]. However, numerical values of the enhancements based on this more accurate expression are only slightly different, so (1) is almost exclusively used.

In conventional SERS, E is averaged over the surface area of the particles where molecules can adsorb to generate the observed enhancement factor $\langle \mathsf{E} \rangle$, while in single-molecule SERS (SMSERS) it is the maximum enhancement $\mathsf{E}_{\max}$ that is of interest. Note that $\mathsf{E}_{\max}$ can be orders of magnitude larger than $\langle \mathsf{E} \rangle$, so the distinction between these two enhancement estimates is important. Another point is that E is often approximated by assuming that $\boldsymbol{E}(\omega)$ and $\boldsymbol{E}(\omega')$ are the same, and hence $\mathsf{E} = |\boldsymbol{E}(\omega)|^4$. This approximation takes advantage of the fact that the plasmon width is often large compared to the Stokes shift. However, in studies of SERS on isolated homogeneous particles, this assumption leads to an overestimate of the enhancement factor by factors of 3 or more.

3 Numerical Methods for Calculating Electromagnetic Enhancement Factors

As noted in the introduction most of the early enhancement-factor estimates were based on analytical theory (either Mie theory for spheres or quasistatic approximations for spheroids). A number of theoretical estimates of SERS enhancement factors have been made in the last few years for nonresonant molecules on nanoparticle surfaces using computational electrodynamics methods such as the discrete dipole approximation (DDA) [59] and the finite difference time-domain (FDTD) [60, 61] method to solve Maxwell's equations to determine the local fields $\boldsymbol{E}(\omega)$. In these methods the particle structures were represented using finite elements so it is not difficult to describe a particle of any shape, and sizes up to a few hundred nm are within standard computational capabilities. These theories can also be used to describe many particles, but ultimately they are limited by the total number of elements needed to converge the calculation. However, it is possible to couple many particles together using coupled multipole expansions.

In the DDA method, one represents the particle by a large number of cubes, each of which is assumed to have a polarizability that is determined by the dielectric constant associated with the cube. If there are N cubes whose positions and polarizabilities are denoted r_i and α_i, then the induced dipole P_i in each particle in the presence of an applied plane wave field is $P_i = \alpha_i E_{\mathrm{loc},i} (i = 1, 2, \ldots, N)$ where the local field $E_{\mathrm{loc}}(r_i)$ is the sum of the incident and retarded fields of the other $N - 1$ dipoles. For a given wavelength λ, this field is:

$$E_{\mathrm{loc},i} = E_{\mathrm{inc},i} + E_{\mathrm{dipole},i} = E_0 \exp(ik \cdot r_i) - \sum_{\substack{j=1 \\ j \neq i}}^{N} A_{ij} \cdot P_j \; i = 1, 2, \ldots, N \,, \quad (2)$$

where E_0 and $k = 2\pi/\lambda$ are the amplitude and wavevector of the incident wave, respectively. The dipole interaction matrix A is expressed as:

$$A_{ij} \cdot P_j = k^2 \mathrm{e}^{ikr_{ij}} \frac{r_{ij} \times (r_{ij} \times P_j)}{r_{ij}^3} + \mathrm{e}^{ikr_{ij}} (1 - ikr_{ij}) \frac{\left[r_{ij}^2 P_j - 3 r_{ij} (r_{ij} \cdot P_j) \right]}{r_{ij}^5}, \quad (i = 1, 2, \ldots, N, j = 1, 2, \ldots, N, j \neq i) \,, \quad (3)$$

where r_{ij} is the vector from dipole i to dipole j. The polarization vectors are obtained by solving $3N$ linear equations of the form

$$\underset{\approx}{A}' \underset{\sim}{P} = \underset{\sim}{E} \,, \quad (4)$$

where the offdiagonal elements of the matrix, A'_{ij}, are the same as A_{ij}, and the diagonal elements of the matrix, A'_{ij}, are α_i^{-1}. Once the induced polarizations have been determined it is relatively easy to obtain fields, and therefore field enhancements, outside the particle using (2) but with all dipoles included in the sum.

The FDTD method is a time-propagation algorithm for solving Maxwell's curl equations on a cubic grid. For a metal in which the dielectric constant is represented via the Drude model

$$\varepsilon_r(\omega) = \varepsilon_\infty - \frac{\omega_\mathrm{p}^2}{\omega^2 + i\omega\gamma} \tag{5}$$

in terms of the plasmon frequency ω_p and width γ, these equations are:

$$\begin{array}{l} \frac{\partial H}{\partial t} = -\frac{1}{\mu_0}\nabla \times E \\ \frac{\partial E}{\partial t} = \frac{1}{\varepsilon_\mathrm{eff}}(\nabla \times H - J), \\ \frac{\partial J}{\partial t} = \varepsilon_0 \omega_p^2 E - \gamma J \end{array} \tag{6}$$

where H, E, J, μ_0, and ε_0 are the magnetic field, electric field, current density, permeability of free space, and permittivity of free space, respectively. The effective dielectric constant is $\varepsilon_\mathrm{eff} = \varepsilon_0\varepsilon_\infty$ if the grid point is inside the metal, and $\varepsilon_\mathrm{eff} = \varepsilon_0$ outside. The finite differencing algorithm was developed by Yee and involves a staggered grid in which the electric- and magnetic-field components are evaluated at half-step intervals from one another both in space and in time. This leads to central-difference approximations to the derivatives that are second order in space and time.

The finite difference equations are solved subject to an initial wavepacket that represents the plane wave incident on the particle. Absorbing boundary conditions are imposed on the edges of the grid to avoid unphysical reflections. The propagation is continued until the wavepacket no longer interacts with the particle, and then the time-dependent field $\boldsymbol{E}(r,t)$ is Fourier transformed to determine the frequency-resolved field that is needed for the SERS enhancement-factor estimate.

4 Results of EM Calculations

Estimates of the SERS enhancements from electrodynamics calculations vary widely depending on what particle structures are used, but for the conventional SERS enhancement, most calculations find that $\langle \mathsf{E} \rangle$ is less than roughly 10^6 [62]. Since this value accounts for most of the observed enhancement factor in conventional SERS (10^6–10^8) this is one reason why it is often assumed that the chemical contribution to the nonresonant SERS enhancement factor is small (less than 10^2) [22]. The story for SMSERS is much less certain. A major problem in making meaningful estimates of SMSERS

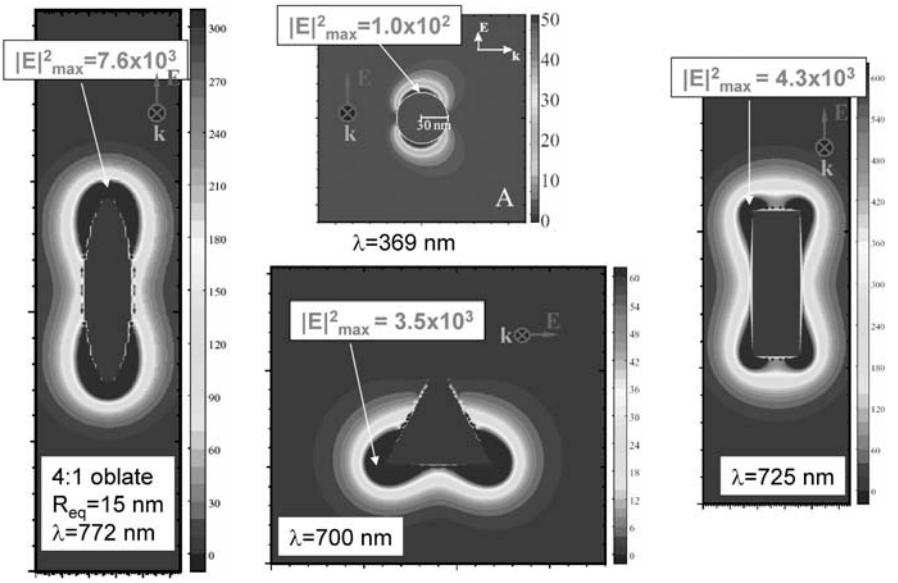

Fig. 1. Contours of the local field near silver particles at specified wavelengths, showing values of the peak field $|\boldsymbol{E}|^2$

enhancement factors is that nearly all SMSERS studies have been done using colloidal aggregates so there are important questions about what aggregate structures are important, and if, as often is the case, the molecule is assumed to be sandwiched between two metal particles, then there are serious problems with the validity of continuum electrodynamics. For isolated particles, the peak $|\boldsymbol{E}|^2$ values for particle sizes and shapes that are commonly studied in experiments are on the order of 10^4 or less, Fig. 1, which suggests enhancement factors of $\mathsf{E}_{\max} = |\boldsymbol{E}|^4 = 10^8$, which is barely above $\langle \mathsf{E} \rangle$. However, larger values, $|\boldsymbol{E}|^4 = 10^{10}$–$10^{11}$ can be obtained for dimers of silver particles, as demonstrated in Fig. 2 [21]. These values, which are associated with the gap between the two nanoparticles, are still below measured estimates of SMSERS enhancement factors (10^{14} or larger [6, 7]) by a factor of 10^3 or more, and this is one reason why it is often thought that SMSERS can only be observed for resonant Raman scatterers. However, this also raises the question as to whether other particle structures might have even larger enhancement factors. We will address this later.

In analyzing these enhancement-factor predictions it is important to note that the key parameter that controls the size of the enhancement factor for a dimer of nanoparticles is the size of the gap between the particles. In calculations by *Hao* and *Schatz* [21], it was found that $\mathsf{E}_{\max}$ varies rapidly with gap size, and it is only for gaps on the order of 1 nm to 2 nm that one can obtain exceptionally large values such as $|\boldsymbol{E}|^4 = 10^{11}$. Unfortunately, this is

just where the reliability of the continuum electrodynamics calculations becomes a problem. One source of error is the use of a local dielectric response model, which is an issue that has occasionally been studied [63], and that always leads to smaller enhancement factors when factored in. In addition, for small particles, or even for large particles that have tips or other complex structures, the influence of scattering of the conduction electrons from the particle surfaces on the dielectric response can result in plasmon broadening that reduces enhancement factors [52]. Although corrections for this have been developed [64, 65, 66] these still use the continuum dielectric response model, so they ultimately fail for small enough particles. Recently, there has been some progress with the development of electronic structure methods for simulating SERS intensities [67, 68] that provides the promise of generating meaningful enhancement factors without using continuum electrodynamics. This will be described later.

5 Long-Range Electromagnetic Enhancement Effects

As noted above, the electromagnetic mechanism of SERS predicts enhancements of up to 10^{11} for a dimer of truncated tetrahedron-shaped particles [21] with a 1 nm gap. Other particle shapes give results that are comparable for optimized sizes, but what was not considered in this analysis is the possibility that large enhancements can be produced by combining the near-field effect considered in Fig. 2 with long-range coupling effects such as one can produce in an aggregate or array of widely spaced particles. There has been some interest in this point in the description of fractal clusters of particles, as here one finds local hot spots due to junction structures in the presence of a large structure that absorbs light efficiently at all wavelengths [8]. Arrays of particles can also be of interest [69, 70], and a particularly exciting possibility involves arrays of junction structures such as dimers of particles.

Figure 3 shows some of the motivation for how an array can influence plasmon excitation, in which we examine the extinction spectrum of a one-dimensional array of 50 nm (radius) spheres, here with the polarization vector and wavevector of the light both perpendicular to the array. The single-sphere extinction spectrum in this case shows a broad peak at about 400 nm that leads to very modest SMSERS enhancements ($\mathsf{E}_{\max} = 10^4$). We see in the figure that for spacings of 450 nm to 500 nm, there are very sharp peaks in the extinction spectrum that arise from long-range dipolar coherent dipolar interactions between the particles [71, 72]. Recent experiments have confirmed this result, although the experimental conditions that lead to the very sharp lines have yet to be achieved [34]. If we examine the SMSERS enhancement for the particles in this array at the resonant wavelengths, we find that $\mathsf{E}_{\max} = 10^6$, indicating that an extra factor of 10^2 is produced as a result of the long-range electrodynamic interactions [70].

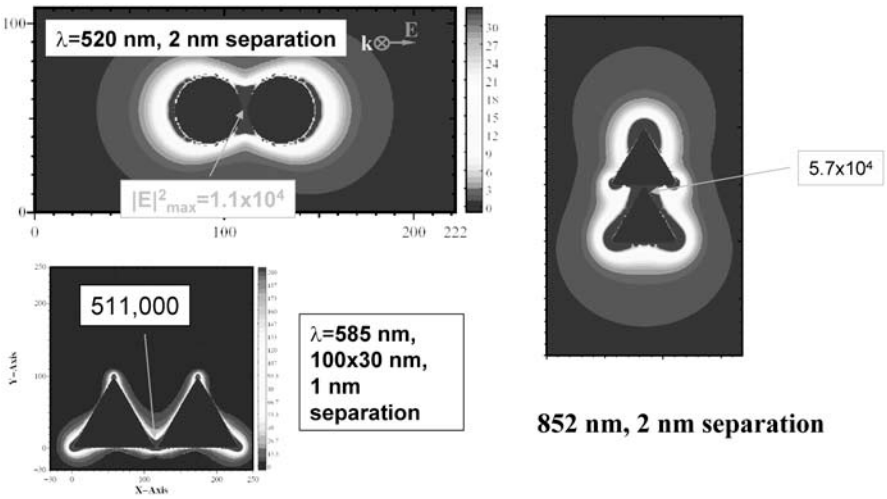

Fig. 2. Contours of the local field near dimers of silver particles at specified wavelengths, showing values of the peak field $|E|^2$

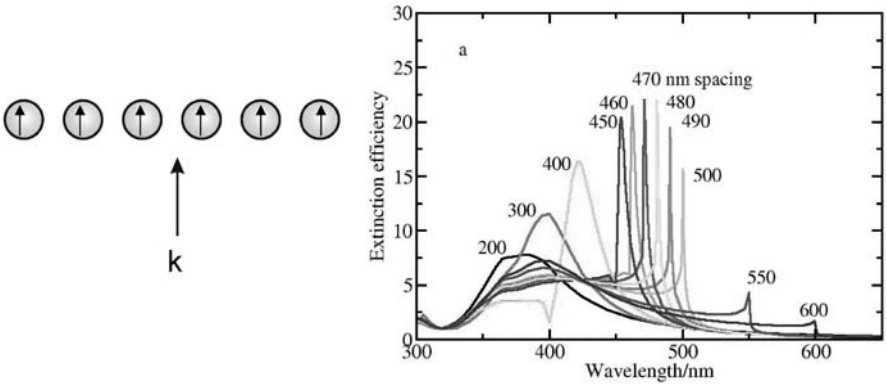

Fig. 3. Extinction spectra associated with an array of 400 silver particles, each with a diameter of 100 nm, for the case where the wavevector and polarization are perpendicular to the array axis. Results are presented for selected nanoparticle separations from 200 nm to 600 nm

Figure 4 shows a simple example of a structure that one might imagine fabricating that would combine the long-range effect just described with short-ranged interactions associated with a junction structure. Here we use an array of dimers of spheres with a spacing that is optimized to produce the highest possible field enhancement from near-field and long-range effects. This particular structure gives $\mathsf{E}_{\max} = 10^9$, but one can construct even better structures by using an array of spheres in which one sphere is replaced

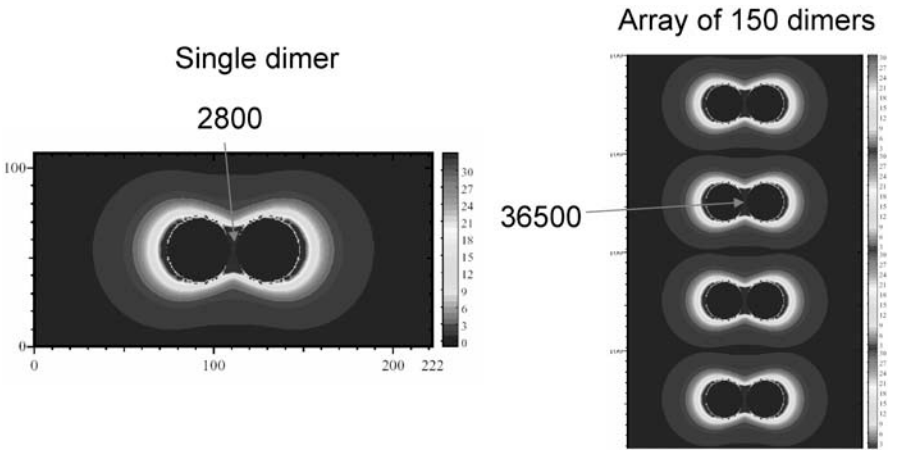

Fig. 4. Field contours for a single dimer of 100 nm diameter silver particles *(left)* at 561 nm (plasmon max), and for an array of 150 dimers *(right)* whose separation is 650 nm at 655 nm

by a dimer of truncated tetrahedrons, leading to SMSERS enhancement estimates of $\mathsf{E}_{\max} = 10^{13}$ [70]. This suggests that enhancements sufficient to generate SMSERS can be achieved without requiring any chemical enhancement. However, there are a number of problems with this analysis, including those mentioned previously concerning the validity of continuum electrodynamics for junctions. In addition, the structure that produces this result is hard to build, involving an array of a large number of spheres that are precisely placed, and with a dimer of specially fabricated particles located in the center of the array. It is also hard to build array structures that produce large electromagnetic enhancements at both the incident and Stokes-shifted wavelengths.

Given these complexities, it is desirable to use theory to identify simpler structures that will still achieve large SMSERS enhancements. One possibility is to generate array structures that allow for long-ranged interactions at multiple wavelengths, thereby removing the problem of generating large electromagnetic enhancements at two wavelengths. For example, the resonances in Fig. 3 that occur for a wavevector perpendicular to the array can also occur when the wavevector is parallel to the array, but for a somewhat different spacing. If one builds two-dimensional arrays that have one spacing in one direction and another spacing in the other direction, then exceptionally large electromagnetic enhancement factors should be possible. (Our preliminary calculations [73] suggest $\mathsf{E}_{\max} = 10^{13-14}$.) A second approach is to combine near-field enhancement from a dimer of metal particles with long-range enhancement that can be produced by dielectric structures. One version of this that has already been done is *Shalaev's* work on SERS from metal-particle aggregates on dielectric tubes in which whispering-gallery mode (WGM) res-

onances were excited [8]. However, WGM resonances tend to be extremely narrow, so this may only give enhancement at one wavelength. Indeed, the enhancement in Raman intensities from WGM excitation in water droplets is a well-known technique that can either be implemented at the incident or Stokes wavelengths, but not both [74,75,76,77,78,79]. An alternative that we have recently modeled [80] is that the near-field region outside a micrometer-size dielectric sphere has a "hot spot" in the forward direction that arises from a simple focusing mechanism. Placing a dimer of metal particles at this hot spot leads to $\mathsf{E}_{\max} = 10^{13}$ under conditions that are relatively easy to achieve.

6 Electronic-Structure Studies

As mentioned earlier there are a number of problems with the use of classical electromagnetic theory to describe SMSERS that make it desirable to develop electronic-structure methods to calculate Raman intensities for molecules adsorbed onto metal particles. This possibility has been of interest for a long time, and there are a large number of electronic-structure studies of the static Raman intensities of molecules [81,82,83,84,85,86,87,88,89,90,91,92,93,94,95,96,97,98,99,100,101], in the presence of silver (or other metal) atoms. However, the calculation of frequency-dependent polarizability derivatives for molecules in the presence of metal particles for frequencies that are onresonance for excitation of the particles has only been considered in a few studies [23,102,103,104,105,106], and only recently have the theoretical methods and computational resources become available to enable meaningful studies of this sort without serious approximations [68]. In these methods, molecule and metal are treated with the same electronic-structure theory, and electron correlation needs to be described well enough to include interband transition effects on the energies of plasmon excitations, and to determine molecular vibrational frequencies and transition moments accurately.

A promising method for doing this is time-dependent density functional theory (TDDFT) based on the Amsterdam density functional (ADF) code [68]. In this version, the finite lifetimes of the excited states of the metal particle are inserted as parameters in the determination of the induced polarization. These are adjusted to match measured extinction spectra or other properties. In a number of applications to metal particles, we find that lifetimes in the range 0.01 eV to 0.10 eV yield accurate absorption spectra.

Figure 5 shows some of the first results of our TDDFT calculations [67], in this case concerned with the resonance polarizability of a 20 atom (1 nm) silver cluster that is pictured in the upper left of the figure. The plot shows both the real and imaginary parts of the polarizability of the cluster as a function of photon energy. The imaginary part of the polarizability is proportional to the extinction cross section, and indeed this looks very much like what would come from a continuum electrodynamics calculation for the same

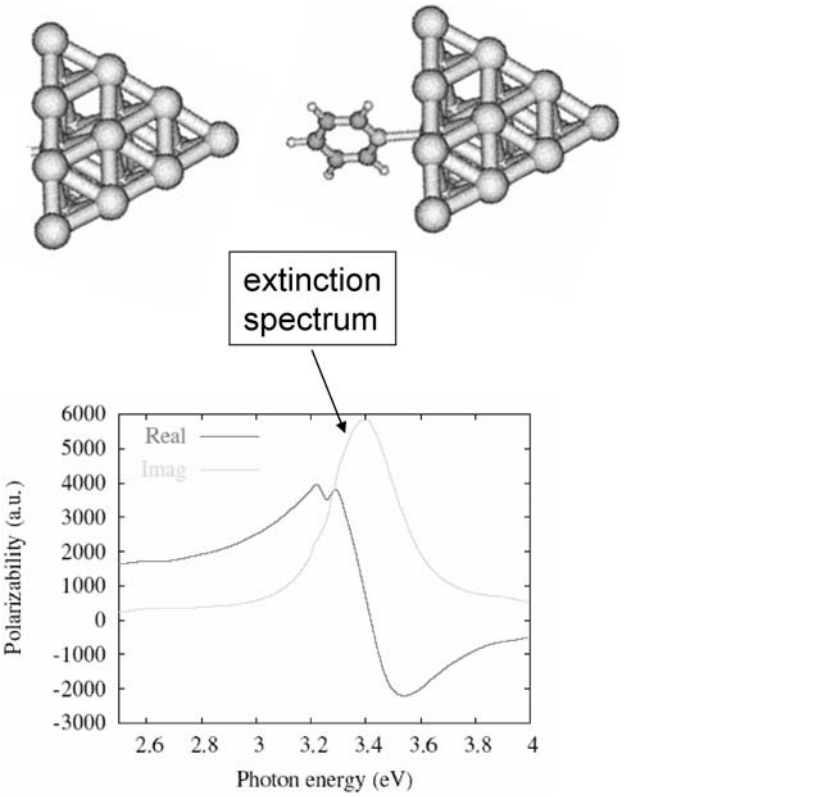

Fig. 5. Structure of 20 atom silver cluster *(upper left)*, and cluster with adsorbed pyridine *(upper right)*. Plot at *bottom* shows the real and imaginary parts of the Ag_{20} polarizability. The imaginary part is proportional to the extinction spectrum

particle using measured dielectric constants as input. In particular, the resonance wavelength is at about 365 nm, which is almost exactly that expected from classical electrodynamics. Of course the peak at 365 nm is not really plasmon excitation in the sense of a collective excitation of all the conduction electrons, however, we find that it consists of a superposition of many excited states, and these states involve many different kinds of excitations (one, two, three, etc., excitations) relative to the ground state.

Perhaps the most important feature of the resonance at 365 nm in Fig. 5 is that this leads to SERS enhancement for molecules interacting with the cluster, such as the pyridine pictured in the upper left of Fig. 5. In Fig. 6 we show TDDFT Raman spectra that we have calculated for pyridine, both as an isolated molecule (left panel) and on the cluster (right panel). The spectra are similar in appearance, but there is a factor of $\mathsf{E} = 10^5$ enhancement in intensity due to the metal cluster. Thus, we find that enhanced Raman is possible for 1 nm clusters, although the effect is smaller than we estimated

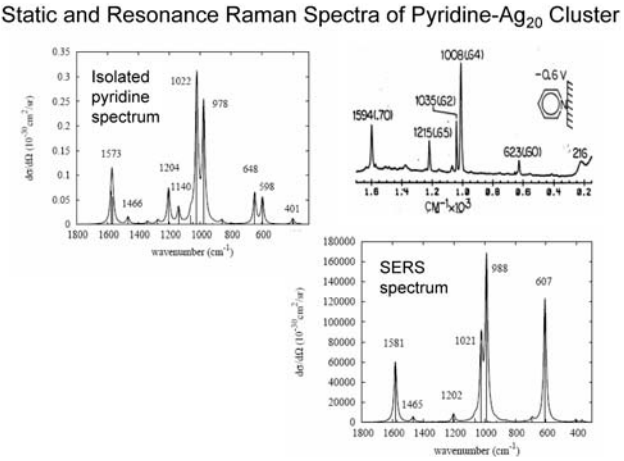

Fig. 6. TDDFT spectrum of pyridine *(left)*, and of the pyridine/Ag_{20} complex *(lower right)*. SERS results from experiment are *upper right*

earlier using classical electrodynamics for larger (>10 nm) particles [22]. The upper trace in Fig. 5 shows a conventional SERS spectrum of pyridine, and we see that this is very close in appearance to what we have calculated.

The results in Fig. 6 can be used as the basis for decomposing the SERS enhancement into chemical and electromagnetic contributions. This work is incomplete, but preliminary results show [107] important electromagnetic and chemical mechanism contributions.

7 SERS Excitation Spectroscopy as a Probe of the Electromagnetic Mechanism

Wavelength-scanned SERES (WS SERES) involves the measurement of SERS enhancement for several laser excitation wavelengths λ_{ex}. This technique was recognized as a useful tool for probing the em mechanism immediately following the discovery of SERS. An obvious limitation of this technique is that the number of data points is determined by the tunability of the excitation laser and detection system. These substantial instrumental requirements have led to the majority of SERES publications suffering from low data point density and/or limited spectral coverage [108, 109, 110, 111, 112]. These limitations prevent the establishment of conclusive generalizations from SERES data. Additionally, most SERES experiments have been performed using surface-enhancing substrates with an unknown or poorly characterized distribution of roughness features. In the few cases where the surfaces are carefully characterized, it is shown that there is a wide distribution of roughness feature sizes [112, 113]. Other studies do not include charac-

terization of the localized surface plasmon resonance (LSPR) of the substrate [108, 109], which prevents any direct comparison of the excitation profiles to the spectral location of the LSPR λ_{max}. The most common substrates historically employed in SERES experiments are Ag-island films and Ag-colloidal solutions. In these cases, the majority of the SERS excitation profiles peak at an excitation wavelength of maximum enhancement ($\lambda_{ex,max}$) near 500 nm to 600 nm [113, 114, 115, 116, 117]. The peaks of the excitation profiles have been shown to shift to longer wavelengths with increased aggregation [111, 113, 115, 116], which is a qualitative result predicted by the electromagnetic enhancement mechanism. With these substrates it is difficult to make a direct comparison between the LSPR of the substrate and the SERS excitation profile because the LSPR of the substrate is a superposition of a wide variety of LSPR wavelengths corresponding to the different roughness features.

Two exceptions to the above statements regarding roughness features are the well-known experiments by *Liao* and coworkers on microlithographically prepared Ag posts [53] and recent work by *Felidj* and coworkers on e-beam lithographically produced arrays of elongated gold nanoparticles [110]. The former ground-breaking work demonstrated excitation profiles where $\lambda_{ex,max}$ shifts to longer wavelengths with increased particle aspect ratio and with increased dielectric constant of the medium surrounding the particles. These results qualitatively agree with the em mechanism, but the LSPR of these substrates was not characterized for a direct comparison. In the latter work, the SERS enhancement was shown to peak at the midpoint between the excitation wavelength and the wavelength of the Raman scattered photon. This important experiment was the first observation of precisely what is predicted by the em mechanism. Unfortunately, this result was obtained on one sample with a profile consisting of three data points.

The limitation of laser and detection tunability has been circumvented by several researchers using a unique approach that involves investigating substrates with variations in the spectral location of the LSPR λ_{max} [118, 119, 120]. These variations allow investigation of the relationship between the LSPR and SERS enhancement using a single excitation wavelength. Our work using plasmon-sampled SERES (PS SERES) on well-defined arrays of nanoparticles was the first systematic study using this technique. PS SERES is a particularly attractive technique from a practical standpoint due to the fact that varying the LSPR λ_{max} of nanoparticles is typically far easier (and more cost effective) than accessing a variety of laser wavelengths. The conclusion of that study was that the condition for maximum enhancement occurred when the peak extinction wavelength of the LSPR, λ_{max}, is located near the midpoint between the energy of laser excitation and the energy of the Raman-scattered photons. This conclusion supports the em mechanism, which predicts that maximum SERS intensity is achieved when the LSPR strongly enhances both the incident and scattered photon intensities. WS SERES allows for a more thorough study of the relationship between the

LSPR and the Raman enhancement, and it affords the advantage of insuring that particle size and shape do not change throughout a given excitation spectrum.

The work described below utilizes a broadly tunable Raman system to measure excitation profiles with the greatest data point density ever demonstrated in a WS SERES experiment. A broadly tunable laser system, a versatile detection system, and a well-characterized surface-enhancing substrate were all employed in order to overcome the traditional shortcomings of WS SERES experiments. The use of a CW-modelocked Ti:sapphire and its harmonics allow for continuous tunability over the spectral ranges 350 nm to 500 nm and 700 nm to 1000 nm. The visible region not covered by the Ti:sapphire system was augmented with the use of a solid-state laser and a tunable dye laser. A triple spectrograph equipped with a CCD camera allows for rapid, multichannel spectral acquisition with efficient rejection of Rayleigh-scattered photons. The SERS substrates used in this work are triangular nanoparticle arrays fabricated by NSL. These substrates present a significant advantage over many of the traditional SERS substrates for SERES studies because NSL-fabricated triangular nanoparticles exhibit extremely narrow size distributions, making them an indispensable tool for probing the fundamental characteristics of SERS. Even though the surface coverage of these nanoparticles is $\sim 7\,\%$, strong SERS intensities are observed from analytes adsorbed to these substrates due to the strong enhancement ($\mathsf{E} \sim 10^8$, vida infra) NSL-fabricated arrays exhibit [118].

For this detailed set of WS SERES experiments performed on optically and topographically characterized SERS substrates, the relative SERS enhancement of the substrates has been shown to vary by three orders of magnitude over the spectral range investigated. It is worth noting that this was not principally a study on the practical application of SERS for chemical analysis. Factors such as spectrograph throughput, detector efficiency, and the ν^4 scattering dependence of Raman photons play an important role in the practice of Raman spectroscopy. Instead, this study was performed in order to contribute fundamental insights into the origins of the SERS effect and to test various aspects of the em mechanism not previously studied. However, the conclusions reached are extremely important for the optimization of a surface-enhanced spectroscopy.

Figure 7 shows a schematic of the instrumentation used for the SERES experiments. All optical measurements were performed using an inverted microscope equipped with a 20× objective (NA = 0.5). The light scattered by the samples was analyzed with a three-stage spectrograph equipped with a liquid-nitrogen-cooled, deep-depletion CCD detector. For the NSL-fabricated triangular nanoparticles, in-situ measurement of the LSPR spectrum was achieved by illuminating the sample with the microscope lamp and analyzing the transmitted light with a fiber-optically coupled miniature spectrometer. It is worthwhile to note that all illumination powers reported in this section were the laser powers incident on the microscope beamsplitter, not the power

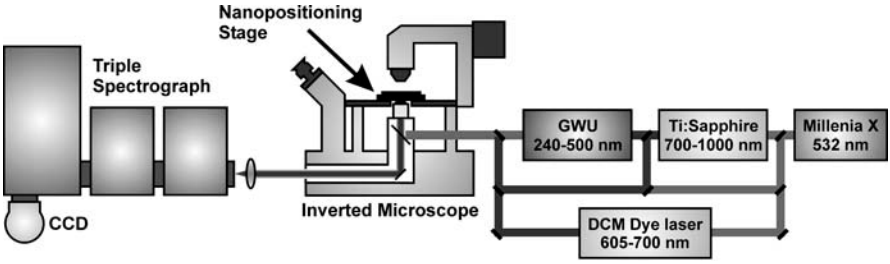

Fig. 7. Schematic diagram of the WS SERES apparatus

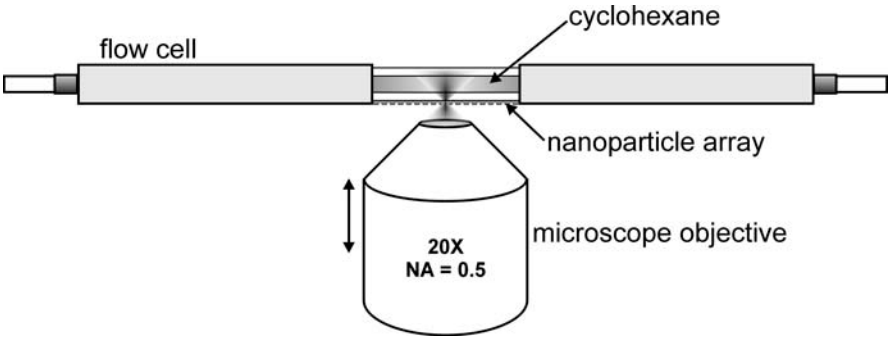

Fig. 8. Schematic diagram of flow cell containing cyclohexane for intensity standard measurements

incident on the sample. Based on experimental measurements, approximately 5 % to 10 % of the reported power is incident on the sample; however, because of the intensity standard the absolute power at the sample is not a critical measurement.

In order to correct for any variation of the SERS intensity not due to the enhancement by the substrate, the 1444 cm^{-1} normal Raman scattering band of neat cyclohexane was used as an intensity standard. This standard was used to correct for the inherent ν^4 behavior of Raman scattering, spectral dependence of the detection system, and differences in the illumination power. This was accomplished by mounting each sample face down as the bottom window of a transparent flow cell. When the flow cell was filled with cyclohexane, the nanoparticle array with an adsorbed benzenethiol monolayer was not in contact with the cyclohexane liquid. In this way, following each SERS acquisition, an intensity standard spectrum of cyclohexane could be taken by translating the inverted microscope objective $\sim 400\,\mu\mathrm{m}$ vertically. A schematic depiction of this setup is shown in Fig. 8.

A representative SERS spectrum of benzenethiol on a Ag-nanoparticle array is shown in Fig. 9. An AFM image of the sample from which this spectrum was taken is shown in the inset. This array was fabricated by depositing

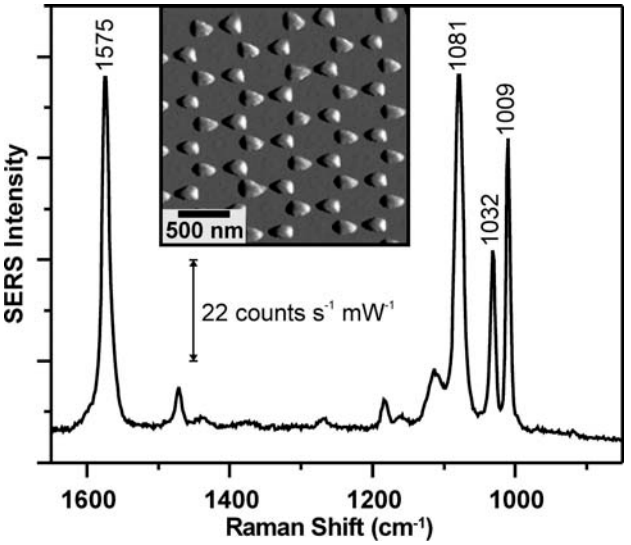

Fig. 9. Representative SERS spectrum of benzenethiol-dosed NSL substrate. $\lambda_{ex} = 620\,\text{nm}$, $P = 3.0\,\text{mW}$, acquisition time $= 150\,\text{s}$. An atomic force micrograph of the sample is shown in the *inset*

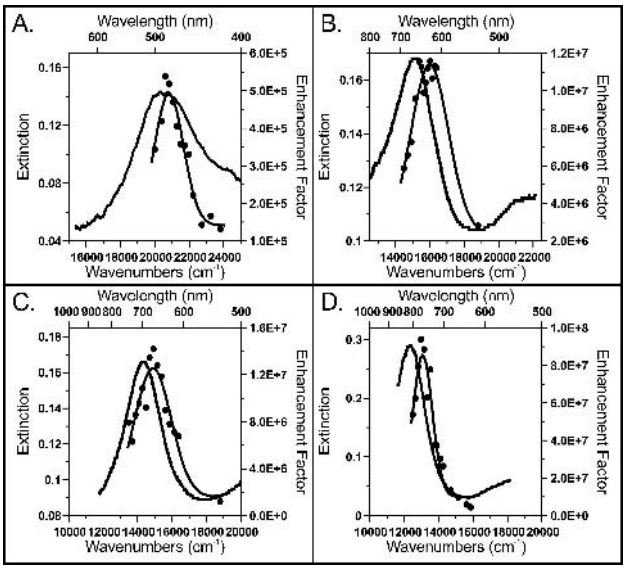

Fig. 10. Surface-enhanced Raman excitation spectra of the $1575\,\text{cm}^{-1}$ peak of benzenethiol with cyclohexane as intensity standard. **(a)** Substrate annealed at 300 °C for 1 h. LSPR $\lambda_{max} = 489\,\text{nm}$, profile fit maximum at $\lambda_{ex,max} = 480\,\text{nm}$. **(b)** LSPR $\lambda_{max} = 663\,\text{nm}$, profile fit maximum at $\lambda_{ex,max} = 625\,\text{nm}$. **(c)** LSPR $\lambda_{max} = 699\,\text{nm}$, profile fit maximum at $\lambda_{ex,max} = 671\,\text{nm}$. **(d)** LSPR $\lambda_{max} = 810\,\text{nm}$, profile fit maximum at $\lambda_{ex,max} = 765\,\text{nm}$

55 nm of Ag through a mask formed with 450 nm diameter nanospheres. Figure 10 shows four excitation profiles for the 1575 cm^{-1} peak of benzenethiol, each with an LSPR λ_{max} at a distinctly different location. The SERES profile in Fig. 10a consists of 13 data points measured over the spectral range 420 nm to 500 nm. Because the formation of a monolayer of benzenethiol on these nanoparticle arrays results in a significant redshift in the position of the LSPR λ_{max}, it was necessary to anneal this sample at 300 °C for 1 h prior to benzenethiol addition in order to achieve a final LSPR λ_{max} at a wavelength shorter than 500 nm. It has been previously shown that annealing NSL-derived samples results in a large blueshift of the LSPR due to changing the shape of the nanoparticles [121]. The LSPR λ_{max} of this substrate was measured to be 489 nm (20 450 cm^{-1}). The largest SERS enhancement occurs at $\lambda_{ex} = 485$ nm. Fitting a Gaussian lineshape to the data reveals that the peak of the excitation profile, $\lambda_{ex,max}$, is 480 nm (20 833 cm^{-1}). The peak E value for this sample was calculated to be 5.5×10^5. This value is low in comparison to the values determined for the other samples because the shape of the nanoparticles is made more ellipsoidal by annealing. In addition to shifting the LSPR λ_{max} to shorter wavelengths, this change decreases the intensity of the electromagnetic fields at the nanoparticle surfaces.

The SERES profile in Fig. 10b consists of 14 data points measured over the spectral range 532 nm to 690 nm. The LSPR λ_{max} of this substrate was measured to be 663 nm (15 083 cm^{-1}). The largest SERS enhancement occurs for $\lambda_{ex} = 625$ nm. The maximum of a Gaussian lineshape fit to the data is 625 nm (16 000 cm^{-1}). The peak E value for this sample is 1.2×10^7. The SERES profile in Fig. 10c consists of 15 data points measured over the spectral range 532 nm to 740 nm. The LSPR λ_{max} of this substrate was measured to be 699 nm (14 306 cm^{-1}). The largest SERS enhancement occurs for $\lambda_{ex} = 670$ nm. The maximum of a Gaussian lineshape fit to the data is 671 nm (14 903 cm^{-1}). The peak E value for this sample is 1.4×10^7. The SERES profile in Fig. 10d consists of 15 data points measured over the spectral range 630 nm to 800 nm. The LSPR λ_{max} of this substrate was measured to be 810 nm (12 346 cm^{-1}). The largest SERS enhancement occurs for $\lambda_{ex} = 770$ nm. The maximum of a Gaussian lineshape fit to the data is 765 nm (13 072 cm^{-1}). The peak E value for this sample is 9.3×10^7.

In order to verify that this behavior can be generalized, two SERES experiments were undertaken in which a different benzenethiol band (1081 cm^{-1}) and intensity standard were monitored. In this case, the intensity standard was the 520 cm^{-1} phonon mode of silicon. The wavelength-dependent absorptivity of silicon requires that the measured Raman intensities must be corrected for differences in laser penetration depth. The penetration depth was calculated at all of the excitation wavelengths using the silicon absorptivities measured by *Aspnes* and *Studna* [122]. The silicon spectra were then normalized so that the intensities were representative of equivalent probe volumes. In addition, a correction was performed to account for the fact that the 520 cm^{-1} band of Si scatters at a significantly different wavelength

from the 1081 cm^{-1} band of benzenethiol, particularly at redder excitation wavelengths. No correction was performed to account for variation in the Raman-scattering cross section of silicon because over the range of excitation wavelengths utilized in this work, the differences in the experimentally determined values of the polarizability of silicon are negligible [123]. The excitation spectra are shown in Fig. 11. The SERES profile in Fig. 11a consists of 13 data points measured over the spectral range 475 nm to 700 nm. The LSPR λ_{max} of this substrate was measured to be 690 nm (14 493 cm^{-1}). The largest SERS enhancement occurs for $\lambda_{ex} = 660$ nm. The maximum of a Gaussian lineshape fit to the data is 662 nm (15 106 cm^{-1}). The peak E value for this sample is 1.9×10^7. The SERES profile in Fig. 11b consists of 17 data points measured over the spectral range 630 nm to 790 nm. The LSPR λ_{max} of this substrate was measured to be 744 nm (13 441 cm^{-1}). The largest relative SERS intensity occurs for $\lambda_{ex} = 700$ nm. The maximum of a Gaussian lineshape fit to the data is 715 nm (13 986 cm^{-1}). The peak E value for this sample is 1.8×10^7.

Each substrate exhibits a SERES profile that has a similar lineshape to the extinction spectrum of the substrate. Also, the $\lambda_{ex,max}$ for the NSL-fabricated substrates is consistently shorter than the LSPR λ_{max}. In all cases, the maximum SERS enhancement occurs when the substrate LSPR λ_{max} is located between λ_{ex} and λ_{vib}. Under these conditions, both the incident and scattered photons experience enhancement by the LSPR. This data is in accordance with the em mechanism of SERS and the experimental work performed previously using PS SERES.

If the peak in the SERS enhancement occurs when the LSPR λ_{max} of the sample is equal to $(\lambda_{ex} + \lambda_{vib})/2$, then $\lambda_{ex,max}$ should be different for the various Raman bands of benzenethiol on a single sample. It is expected that $\lambda_{ex,max}$ will have a larger separation from the LSPR λ_{max} for a large Raman shift than for a small shift. Excitation profiles for three benzenethiol peaks on a single substrate are shown in Fig. 12. For this substrate, the LSPR λ_{max} is 729 nm. Figure 12a shows the SERS excitation profile for the 1575 cm^{-1} peak of benzenethiol, normalized to the 1444 cm^{-1} peak of liquid cyclohexane. The separation in wave numbers between the LSPR λ_{max} and $\lambda_{ex,max}$ is 734 cm^{-1}. In Fig. 12b, the excitation profile for the 1081 cm^{-1} benzenethiol peak (normalized to the 1028 cm^{-1} peak of cyclohexane) is shown. The separation in wave numbers between the LSPR λ_{max} and $\lambda_{ex,max}$ is 569 cm^{-1}. Finally, in Fig. 12c, the excitation profile for the 1009 cm^{-1} benzenethiol peak (normalized to the 1028 cm^{-1} peak of cyclohexane) is shown, and the separation in wave numbers between the LSPR λ_{max} and $\lambda_{ex,max}$ is 488 cm^{-1}. This data demonstrates the qualitative trend whereby the $\lambda_{ex,max}$ in the excitation spectra of larger Raman-shifted bands yield a larger separation from the LSPR λ_{max} than those of smaller Raman-shifted bands, and this once again lends support to the electromagnetic mechanism.

Previous work has demonstrated that the spectral location of the LSPR is extremely sensitive to the presence of molecular adsorbates [26, 124, 125].

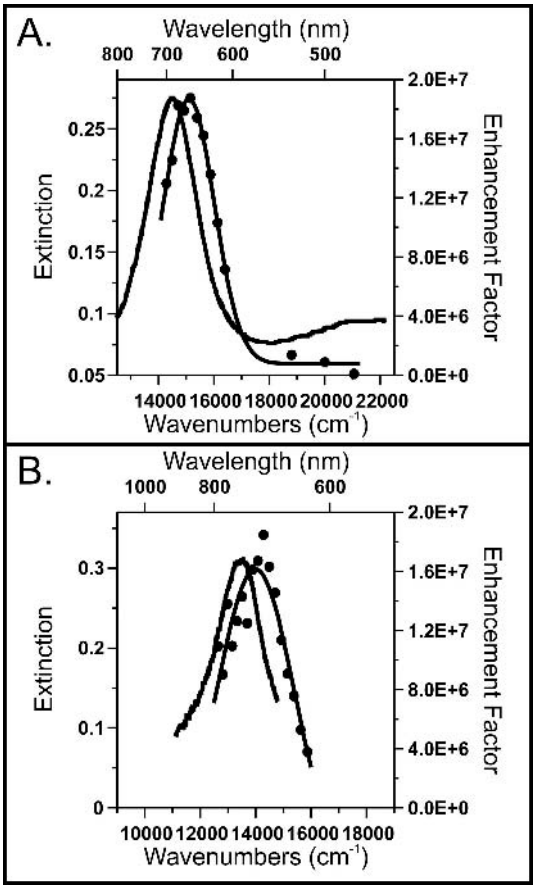

Fig. 11. Surface-enhanced Raman excitation spectra of the $1081\,\mathrm{cm}^{-1}$ peak of benzenethiol with Si as intensity standard. **(a)** LSPR $\lambda_{\max} = 690\,\mathrm{nm}$, profile fit maximum at $\lambda_{\mathrm{ex,max}} = 662\,\mathrm{nm}$. **(b)** LSPR $\lambda_{\max} = 744\,\mathrm{nm}$, profile fit maximum at $\lambda_{\mathrm{ex,max}} = 715\,\mathrm{nm}$

Therefore, it is important to note that the relationship between the LSPR spectra and SERES profiles depicted in Fig. 10, Fig. 11 and Fig. 12 pertain to LSPR spectra measured after adsorption of the analyte molecule. Figure 13 demonstrates the importance of considering this point. For a bare nanoparticle array, the LSPR $\lambda_{\max}$ was measured to be 672 nm. After incubation in 1 mM benzenethiol for > 3 h, thorough rinsing with methanol, and drying, the LSPR $\lambda_{\max}$ was observed to have redshifted by 57 nm to 729 nm. Measurement of the WS SERES profile yields $\lambda_{\mathrm{ex,max}} = 692\,\mathrm{nm}$. This is blueshifted with respect to the LSPR $\lambda_{\max}$ of the adsorbate-covered sample, as observed for the other samples used in this study, but redshifted with respect to the LSPR $\lambda_{\max}$ of the bare nanoparticle array. This demonstrates that it is criti-

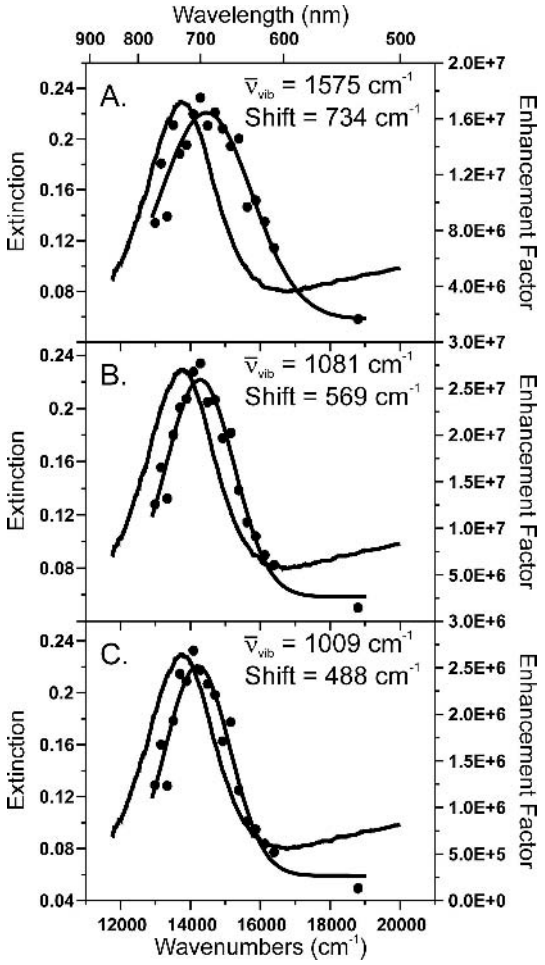

Fig. 12. Effect of Stokes Raman shift. (**a**) Profile of the 1575 cm^{-1} vibrational mode of benzenethiol. Distance between LSPR λ_{max} and excitation profile fit line $\lambda_{ex,max}$ = 734 cm^{-1}. E = 1.8×10^7. (**b**) 1081 cm^{-1} vibrational mode, shift = 569 cm^{-1}, E = 2.8×10^7. (**c**) 1009 cm^{-1} vibrational mode, shift = 488 cm^{-1}, E = 2.7×10^6

cal to characterize the LSPR of a SERS substrate after analyte adsorption in order to choose the appropriate laser excitation wavelength for maximizing E or to draw any conclusions about the fundamental mechanism of the SERS effect.

This work demonstrates the most thorough WS SERES experiments ever performed on optically and topographically characterized SERS substrates. The experimental apparatus utilized has proven effective for the measurement of relative SERS enhancements that vary by three orders of magnitude. This

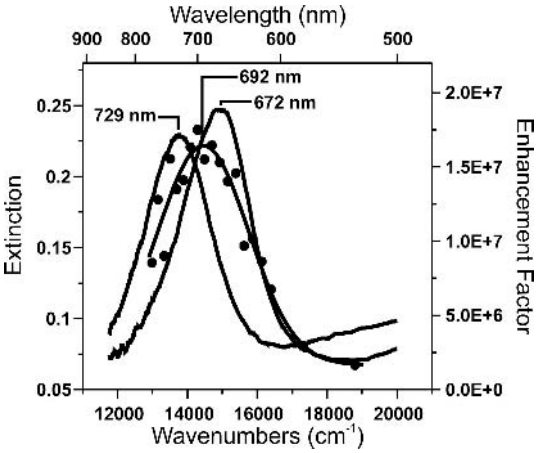

Fig. 13. LSPR shift and SERES profile for the $1575\,\mathrm{cm}^{-1}$ peak of benzenethiol. The line with $\lambda_{\max} = 672\,\mathrm{nm}$ is the LSPR extinction of the bare nanoparticle array. The line with $\lambda_{\max} = 729\,\mathrm{nm}$ is the LSPR extinction of the nanoparticle array with an adsorbed monolayer of benzenethiol. The line with $\lambda_{\mathrm{ex,max}} = 692\,\mathrm{nm}$ is the best fit to the SERES data points

work demonstrates that the relationship between the substrate LSPR and the SERES profile for size-homogenous nanoparticles is consistent throughout the visible range. In all cases the experimentally observed behavior is consistent with that predicted by the em mechanism. Specifically, the strongest SERS enhancement occurs under conditions where the incident and Raman scattered photons are both strongly enhanced. The largest E measured was $\sim 10^8$ for the triangular nanoparticle arrays studied. Ultimately, refinement of the experimental apparatus and optimization of SERS enhancement will allow SERES to be performed using single-nanoparticle substrates. This level provides the best possible case in terms of reducing sample heterogeneity. These experiments are expected to provide key information to validate the em mechanism of SERS and will present an additional technique that can be used to study the SMSERS effect.

8 Conclusions

Using electrodynamics calculations, predicted E values as large as 10^{11} have been shown for nanoparticle dimers with small (1 nm to 2 nm) gaps. An E value of 10^{13} can be achieved with an array of dimers of truncated tetrahedra. This suggests that it is at least theoretically possible to realize an enhancement sufficient to generate SMSERS without appealing to any chemical enhancement. Because the structures required to produce the largest

enhancements are difficult to build and unlikely to be what is occurring in experimental SMSERS, other simpler structures have also been explored.

To overcome the difficulties associated with using classical electromagnetic theory to model SERS for small nanoparticles with very small gaps, electronic structure methods are being developed for use in this area. Preliminary TDDFT calculations have shown good agreement with experiment for the SERS spectrum of pyridine. This method can be used to decompose the SERS enhancement into chemical and electromagnetic contributions, and the first results have shown important contributions from both sources.

The WS SERES results reviewed herein are the most detailed ever performed on optically and topographically characterized SERS substrates. The SERS enhancement factor has been shown to vary significantly as a function of laser wavelength for substrates with LSPR $\lambda_{\max}$ values throughout the visible spectrum. The consistent conclusion, verifying the electromagnetic mechanism prediction, is that the SERS enhancement factor is maximized when both the incident laser and Raman-scattered photons are strongly enhanced. This occurs when the incident laser is on the higher-energy side of $\lambda_{\max}$, and the Raman shift is on the lower-energy side. Additionally, the electromagnetic mechanism prediction concerning the effect of the Stokes shift on SERES has been verified. Specifically, the data demonstrates that a peak with a smaller Raman shift shows a maximum enhancement closer in energy to the LSPR $\lambda_{\max}$ than a peak with a larger Raman shift. The conditions for maximum SERS enhancement are determined after the addition of the analyte molecule because of the significant shift in the LSPR $\lambda_{\max}$ caused by analyte adsorption. The adsorbate-induced LSPR shift and SERES Stokes shift are in opposite directions. The largest E measured was $\sim 10^8$ for the triangular nanoparticle arrays studied, which is in accordance with theory and previous experimental work.

Acknowledgements

The authors gratefully acknowledge support from the Air Force Office of Scientific Research MURI program (Grant F49620-02-1-0381) and the National Science Foundation (EEC-0118025, DMR-0076097, CHE-0414554, DGE-0114429).

References

[1] M. Fleischmann, P. J. Hendra, A. J. Mcquillan: Chem. Phys. Lett. **26**, 163 (1974)
[2] D. L. Jeanmaire, R. P. Van Duyne: J. Electroanal. Chem. Interf. Electrochem. **84**, 1 (1977)
[3] C. L. Haynes, A. D. McFarland, R. P. Van Duyne: Anal. Chem. **77**, 338A (2005)

[4] C. R. Yonzon, C. L. Haynes, X. Zhang, J. T. Walsh, Jr., R. P. Van Duyne: Anal. Chem. **76**, 78 (2004)
[5] O. Lyandres, N. C. Shah, C. R. Yonzon, J. T. Walsh Jr., M. R. Glucksberg, R. P. Van Duyne: Anal. Chem. **77**, 6134 (2005)
[6] K. Kneipp, Y. Wang, H. Kneipp, L. T. Perelman, I. Itzkan, R. R. Dasari, M. S. Feld: Phys. Rev. Lett. **78**, 1667 (1997)
[7] S. Nie, S. R. Emory: Science **275**, 1102 (1997)
[8] W. Kim, V. P. Safonov, V. M. Shalaev, R. L. Armstrong: Phys. Rev. Lett. **82**, 4811 (1999)
[9] L. Cui, Z. Liu, S. Duan, D.-Y. Wu, B. Ren, Z.-Q. Tian, S.-Z. Zou: J. Phys. Chem. B **109**, 17597 (2005)
[10] X.-F. Lin, B. Ren, Z.-Q. Tian: J. Phys. Chem. B **108**, 981 (2004)
[11] B. Ren, X.-F. Lin, Z.-L. Yang, G.-K. Liu, R. F. Aroca, B.-W. Mao, Z.-Q. Tian: J. Am. Chem. Soc. **125**, 9598 (2003)
[12] B. Ren, X.-F. Lin, J.-W. Yan, B.-W. Mao, Z.-Q. Tian: J. Phys. Chem. B **107**, 899 (2003)
[13] J.-Z. Zheng, B. Ren, D.-Y. Wu, Z.-Q. Tian: J. Electroanal. Chem. **574**, 285 (2005)
[14] S. A. Bilmes, J. C. Rubim, A. Otto, A. J. Arvia: Chem. Phys. Lett. **159**, 89 (1989)
[15] M. A. Bryant, S. L. Joa, J. E. Pemberton: Langmuir **8**, 753 (1992)
[16] P. Cao, Y. Sun, R. Gu: J. Phys. Chem. B **108**, 4716 (2004)
[17] R. Gomez, J. Solla-Gullon, J. M. Perez, A. Aldaz: Chem. Phys. Chem. **6**, 2017 (2005)
[18] Y. Kim, R. C. Johnson, J. T. Hupp: Nano Lett. **1**, 165 (2001)
[19] J. Miragliotta, T. E. Furtak: Mater. Res. Soc. Symp. Proc. **83**, 123 (1987)
[20] M. Muniz-Miranda: J. Raman Spectrosc. **27**, 435 (1996)
[21] E. Hao, G. C. Schatz: J. Chem. Phys. **120**, 357 (2004)
[22] G. C. Schatz, R. P. Van Duyne: Electromagnetic mechanism of surface enhanced spectroscopy, in J. M. Chalmers, P. R. Griffiths (Eds.): *Handbook of Vibrational Spectroscopy* (Wiley, Chichester 2002) p. 759
[23] S. Corni, J. Tomasi: Chem. Phys. Lett. **342**, 135 (2001)
[24] T. R. Jensen, M. L. Duval, K. L. Kelly, A. A. Lazarides, G. C. Schatz, R. P. Van Duyne: J. Phys. Chem. B **103**, 9846 (1999)
[25] T. R. Jensen, G. C. Schatz, R. P. Van Duyne: J. Phys. Chem. B **103**, 2394 (1999)
[26] M. D. Malinsky, K. L. Kelly, G. C. Schatz, R. P. Van Duyne: J. Am. Chem. Soc. **123**, 1471 (2001)
[27] C. L. Haynes, A. D. McFarland, L. Zhao, R. P. Van Duyne, G. C. Schatz, L. Gunnarsson, J. Prikulis, B. Kasemo, M. Kaell: J. Phys. Chem. B **107**, 7337 (2003)
[28] A. J. Haes, S. Zou, G. C. Schatz, R. P. Van Duyne: J. Phys. Chem. B **108**, 6961 (2004)
[29] A. J. Haes, S. Zou, G. C. Schatz, R. P. Van Duyne: J. Phys. Chem. B **108**, 109 (2004)
[30] C. R. Yonzon, E. Jeoung, S. Zou, G. C. Schatz, M. Mrksich, R. P. Van Duyne: J. Am. Chem. Soc. **126**, 12669 (2004)
[31] A. J. Haes, C. L. Haynes, A. D. McFarland, G. C. Schatz, R. P. van Duyne, S. Zou: MRS Bull. **30**, 368 (2005)

[32] A. J. Haes, J. Zhao, S. Zou, C. S. Own, L. D. Marks, G. C. Schatz, R. P. Van Duyne: J. Phys. Chem. B **109**, 11158 (2005)
[33] E. M. Hicks, X. Zhang, S. Zou, O. Lyandres, K. G. Spears, G. C. Schatz, R. P. Van Duyne: J. Phys. Chem. B **109**, 22351 (2005)
[34] E. M. Hicks, S. Zou, G. C. Schatz, K. G. Spears, R. P. Van Duyne, L. Gunnarsson, T. Rindzevicius, B. Kasemo, M. Kaell: Nano Lett. **5**, 1065 (2005)
[35] L. J. Sherry, S.-H. Chang, G. C. Schatz, R. P. Van Duyne, B. J. Wiley, Y. Xia: Nano Lett. **5**, 2034 (2005)
[36] X. Zhang, E. M. Hicks, J. Zhao, G. C. Schatz, R. P. Van Duyne: Nano Lett. **5**, 1503 (2005)
[37] P. K. Aravind, A. Nitzan, H. Metiu: Surf. Science **110**, 189 (1981)
[38] S. Efrima: J. Phys. Chem. **89**, 2843 (1985)
[39] P. J. Feibelman: Phys. rev. b, Condens. Matter Mater. Phys. **22**, 3654 (1980)
[40] J. Gersten, A. Nitzan: J. Chem. Phys. **73**, 3023 (1980)
[41] R. M. Hexter, M. G. Albrecht: Spectrochim. acta, part a, Molec. Biomol. Spectrosc. **233**, 35A (1979)
[42] M. Kerker, O. Siiman, L. A. Bumm, D. S. Wang: Appl. Opt. **19**, 3253 (1980)
[43] F. W. King, R. P. Van Duyne, G. C. Schatz: J. Chem. Phys. **69**, 4472 (1978)
[44] M. Moskovits: Solid State Commun. **32**, 59 (1979)
[45] A. Wokaun, J. P. Gordon, P. F. Liao: Phys. Rev. Lett. **48**, 957 (1982)
[46] H. Metiu, P. Das: Ann. Rev. Phys. Chem. **35**, 507 (1984)
[47] G. C. Schatz: Acc. Chem. Res. **17**, 370 (1984)
[48] M. Moskovits: Rev. Mod. Phys. **57**, 783 (1985)
[49] M. R. Philpott: J. Chem. Phys. **61**, 5306 (1974)
[50] M. Moskovits: J. Chem. Phys. **69**, 4159 (1978)
[51] D. S. Wang, H. Chew, M. Kerker: Appl. Opt. **19**, 2256 (1980)
[52] E. J. Zeman, G. C. Schatz: J. Phys. Chem. **91**, 634 (1987)
[53] P. F. Liao, J. G. Bergman, D. S. Chemla, A. Wokaun, J. Melngailis, A. M. Hawryluk, N. P. Economou: Chem. Phys. Lett. **82**, 355 (1981)
[54] M. Kerker: Studies Phys. Theoret. Chem. **45**, 3 (1987)
[55] M. R. Philpott: Colloque, J. Phys. **C10**, 295 (1983)
[56] A. Wokaun: Solid State Phys. **38**, 223 (1984)
[57] A. Wokaun: Molec. Phys. **56**, 1 (1985)
[58] M. Kerker: J. Colloid Interf. Sci. **118**, 417 (1987)
[59] W.-H. Yang, G. C. Schatz, R. P. Van Duyne: J. Chem. Phys. **103**, 869 (1995)
[60] A. Taflove, S. C. Hagness: *The Finite-Difference Time-Domain Method* (Artech House Inc., Norwood, MA 2005)
[61] L. Yin, V. K. Vlasko-Vlasov, A. Rydh, J. Pearson, U. Welp, S.-H. Chang, S. K. Gray, G. C. Schatz, D. E. Brown, C. W. Kimball: Appl. Phys. Lett. **85**, 467 (2004) Los Alamos National Laboratory, Preprint Archive
[62] K. L. Kelly, T. R. Jensen, A. A. Lazarides, G. C. Schatz: Modeling metal nanoparticles optical properties, in D. Feldheim, C. Foss (Eds.): *Metal Nanoparticles: Synthesis, Characterization and Applications* (Marcel-Dekker, New York 2002) p. 89
[63] P. T. Leung, W. S. Tse: Solid State Commun. **95**, 39 (1995)
[64] E. A. Coronado, G. C. Schatz: J. Chem. Phys. **119**, 3926 (2003)
[65] A. Hilger, T. von Hofe, U. Kreibig: Nova Acta Leopoldina **92**, 9 (2005)

[66] A. Reinholdt, R. Pecenka, A. Pinchuk, S. Runte, A. L. Stepanov, T. E. Weirich, U. Kreibig: European Phys. J. D, At. Molec. Opt. Phys. **31**, 69 (2004)
[67] L. Zhao, L. Jensen, G. C. Schatz: J. Am. Chem. Soc. **128**, 2911 (2006)
[68] L. Jensen, J. Autschbach, G. C. Schatz: J. Chem. Phys. **122**, 224115/1 (2005)
[69] D. A. Genov, A. K. Sarychev, V. M. Shalaev, A. Wei: Nano Lett. **4**, 153 (2004)
[70] S. Zou, G. C. Schatz: Chem. Phys. Lett. **403**, 62 (2005)
[71] S. Zou, N. Janel, G. C. Schatz: J. Chem. Phys. **120**, 10871 (2004)
[72] S. Zou, G. C. Schatz: J. Chem. Phys. **122**, 097102/1 (2005)
[73] S. Zou, G. C. Schatz: Coupled plasmonic plasmon/photonic resonance effects in sers, in K. Kneipp, M. Moskovitz, H. Kneipp (Eds.): *Surface Enhanced Raman Scattering: Physics and Applications* (Springer, Berlin 2006) p. 67
[74] R. Symes, R. J. J. Gilham, R. M. Sayer, J. P. Reid: Phys. Chem. Chem. Phys. **7**, 1414 (2005)
[75] R. Symes, R. M. Sayer, J. P. Reid: Phys. Chem. Chem. Phys. **6**, 474 (2004)
[76] J. F. Widmann, C. L. Aardahl, E. J. Davis: TrAC, Trends Anal. Chem. **17**, 339 (1998)
[77] E. J. Davis, C. L. Aardahl, J. F. Widmann: J. Dispers. Sci. Technol. **19**, 293 (1998)
[78] C. L. Aardahl, W. R. Foss, E. J. Davis: J. Aerosol Sci. **27**, 1015 (1996)
[79] K. Schaschek, J. Popp, W. Kiefer: J. Raman Spectrosc. **24**, 69 (1993)
[80] S. Zou, G. C. Schatz: Israel J. Chem. (2006)
[81] W.-H. Yang, J. Hulteen, G. C. Schatz, R. P. Van Duyne: J. Chem. Phys. **104**, 4313 (1996)
[82] R. F. Aroca, R. E. Clavijo, M. D. Halls, H. B. Schlegel: J. Phys. Chem. A **104**, 9500 (2000)
[83] T. Iliescu, M. Bolboaca, R. Pacurariu, D. Maniu, W. Kiefer: J. Raman Spectrosc. **34**, 705 (2003)
[84] P. E. Schoen, R. G. Priest, J. P. Sheridan, J. M. Schnur: Nature **270**, 412 (1977)
[85] E. A. Carrasco Flores, M. M. Campos Vallette, R. E. C. Clavijo, P. Leyton, G. Diaz F, R. Koch: Vibrat. Spectrosc. **37**, 153 (2005)
[86] K.-H. Cho, J. Choo, S.-W. Joo: J. Molec. Struct. **738**, 9 (2005)
[87] T. Iliescu, D. Maniu, V. Chis, F. D. Irimie, C. Paizs, M. Tosa: Chem. Phys. **310**, 189 (2005)
[88] A. V. Szeghalmi, L. Leopold, S. Pinzaru, V. Chis, I. Silaghi-Dumitrescu, M. Schmitt, J. Popp, W. Kiefer: Biopolymers **78**, 298 (2005)
[89] S. Thomas, N. Biswas, S. Venkateswaran, S. Kapoor, R. D'Cunha, T. Mukherjee: Chem. Phys. Lett. **402**, 361 (2005)
[90] S. Naumov, S. Kapoor, S. Thomas, S. Venkateswaran, T. Mukherjee: Theochem. **685**, 127 (2004)
[91] M. Baia, L. Baia, W. Kiefer, J. Popp: J. Phys. Chem. B **108**, 17491 (2004)
[92] G. Cardini, M. Muniz-Miranda, V. Schettino: J. Phys. Chem. B **108**, 17007 (2004)
[93] S. D. Silaghi, G. Salvan, M. Friedrich, T. U. Kampen, R. Scholz, D. R. T. Zahn: Appl. Surf. Sci. **235**, 73 (2004)
[94] S. Cinta Pinzaru, N. Leopold, I. Pavel, W. Kiefer: Spectrochim. acta, part a, Molec. Biomolec. Spectrosc. **60A**, 2021 (2004)

[95] T. Iliescu, M. Baia, I. Pavel: J. Raman Spect. **37**, 318 (2006)
[96] B. Pergolese, M. Muniz-Miranda, G. Sbrana, A. Bigotto: Far. Disc. **132**, 111 (2006)
[97] T. Tanaka, A. Nakajima, A. Watanabe, T. Ohno, Y. Ozaki: Vibrat. Spectrosc. **34**, 157 (2004)
[98] T. Tanaka, A. Nakajima, A. Watanabe, T. Ohno, Y. Ozaki: J. Molec. Struct. **661–662**, 437 (2003)
[99] B. Giese, D. McNaughton: Biopolymers **72**, 472 (2003)
[100] D.-Y. Wu, B. Ren, X. Xu, G.-K. Liu, Z.-L. Yang, Z.-Q. Tian: J. Chem. Phys. **119**, 1701 (2003)
[101] M. Bolboaca, T. Iliescu, C. Paizs, F. D. Irimie, W. Kiefer: J. Phys. Chem. A **107**, 5144 (2003)
[102] P. K. K. Pandey, G. C. Schatz: J. Chem. Phys. **80**, 2959 (1984)
[103] H. Nakai, H. Nakatsuji: J. Chem. Phys. **103**, 2286 (1995)
[104] S. Corni, J. Tomasi: J. Chem. Phys. **114**, 3739 (2001)
[105] S. Corni, J. Tomasi: Chem. Phys. Lett. **365**, 552 (2002)
[106] S. Corni, J. Tomasi: J. Chem. Phys. **116**, 1156 (2002)
[107] L. Zhao, L. Jensen, G. C. Schatz: Nano Lettres **6** (2006) in press
[108] B. Vlckova, X. J. Gu, M. Moskovits: J. Phys. Chem. B **101**, 1588 (1997)
[109] B. W. Gregory, B. K. Clark, J. M. Standard, A. Avila: J. Phys. Chem. B **105**, 4684 (2001)
[110] N. Felidj, J. Aubard, G. Levi, J. R. Krenn, A. Hohenau, G. Schider, A. Leitner, F. R. Aussenegg: Appl. Phys. Lett. **82**, 3095 (2003)
[111] C. G. Blatchford, J. R. Campbell, J. A. Creighton: Surf. Sci. **120**, 435 (1982)
[112] R. P. Van Duyne, J. C. Hulteen, D. A. Treichel: J. Chem. Phys. **99**, 2101 (1993)
[113] K. U. Von Raben, R. K. Chang, B. L. Laube, P. W. Barber: J. Phys. Chem. **88**, 5290 (1984)
[114] D. A. Weitz, S. Garoff, T. J. Gramila: Opt. Lett. **7**, 168 (1982)
[115] M. Kerker, O. Siiman, D. S. Wang: J. Phys. Chem. **88**, 3168 (1984)
[116] D. Fornasiero, F. Grieser: J. Chem. Phys. **87**, 3213 (1987)
[117] H. Feilchenfeld, O. Siiman: J. Phys. Chem. **90**, 2163 (1986)
[118] C. L. Haynes, R. P. Van Duyne: J. Phys. Chem. B **107**, 7426 (2003)
[119] W. A. Weimer, M. J. Dyer: Appl. Phys. Lett. **79**, 3164 (2001)
[120] S. J. Oldenburg, S. L. Westcott, R. D. Averitt, N. J. Halas: J. Chem. Phys. **111**, 4729 (1999)
[121] T. R. Jensen, M. D. Malinsky, C. L. Haynes, R. P. van Duyne: J. Phys. Chem. B **104**, 10549 (2000)
[122] D. E. Aspnes, A. A. Studna: Phys. Rev. B, Condens Matter Mater. Phys. **27**, 985 (1983)
[123] M. Grimsditch, M. Cardona: Basic Research, Phys. Stat. Solidi B **102**, 155 (1980)
[124] A. D. McFarland, R. P. Van Duyne: Nano Lett. **3**, 1057 (2003)
[125] A. J. Haes, R. P. Van Duyne: J. Am. Chem. Soc. **124**, 10596 (2002)

Index